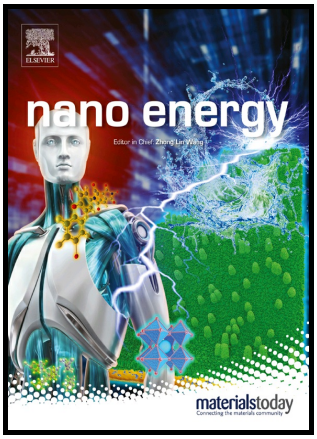

Rational Band Engineering and Structural Manipulations Inducing High Thermoelectric Performance in n-Type $CoSb_3$ Thin Films

Zhuang-Hao Zheng, Xiao-Lei Shi, Dong-Wei Ao, Wei-Di Liu, Yue-Xing Chen, Fu Li, Shuo Chen, Xiao-Qing Tian, Xin-Ru Li, Jing-Yi Duan, Hong-Li Ma, Xiang-Hua Zhang, Guang-Xing Liang, Ping Fan, Zhi-Gang Chen

PII: S2211-2855(20)31256-8

DOI: https://doi.org/10.1016/j.nanoen.2020.105683

Reference: NANOEN105683

To appear in: *Nano Energy*

Received date: 9 September 2020
Revised date: 13 November 2020
Accepted date: 9 December 2020

Please cite this article as: Zhuang-Hao Zheng, Xiao-Lei Shi, Dong-Wei Ao, Wei-Di Liu, Yue-Xing Chen, Fu Li, Shuo Chen, Xiao-Qing Tian, Xin-Ru Li, Jing-Yi Duan, Hong-Li Ma, Xiang-Hua Zhang, Guang-Xing Liang, Ping Fan and Zhi-Gang Chen, Rational Band Engineering and Structural Manipulations Inducing High Thermoelectric Performance in n-Type $CoSb_3$ Thin Films, *Nano Energy,* (2020) doi:https://doi.org/10.1016/j.nanoen.2020.105683

Rational Band Engineering and Structural Manipulations Inducing High Thermoelectric Performance in n-Type $CoSb_3$ Thin Films

Zhuang-Hao Zheng [a,b,*,#], *Xiao-Lei Shi* [b,c,#], *Dong-Wei Ao* [a,d,#], *Wei-Di Liu* [b,c], *Yue-Xing Chen* [a], *Fu Li* [a], *Shuo Chen* [a], *Xiao-Qing Tian* [a], *Xin-Ru Li* [a], *Jing-Yi Duan* [a], *Hong-Li Ma* [d], *Xiang-Hua Zhang* [d], *Guang-Xing Liang* [a,], *Ping Fan* [a,*] *and Zhi-Gang Chen* [b,c,*]

[a] Shenzhen Key Laboratory of Advanced Thin Films and Applications, Key Laboratory of Optoelectronic Devices and Systems of Ministry of Education and Guangdong Province, College of Physics and Optoelectronic Engineering, Shenzhen University, Shenzhen 518060, P. R. China;

[b] Centre for Future Materials, University of Southern Queensland, Springfield Central, Brisbane, Queensland 4300, Australia;

[c] School of Mechanical and Mining Engineering, The University of Queensland, St Lucia, Brisbane, Queensland 4072, Australia;

[d] Univ Rennes, CNRS, ISCR (Institut des Sciences Chimiques de Rennes) UMR6226, Rennes F-35000, France.

[*] Corresponding authors E-mail: zhengzh@szu.edu.cn (ZHZ), fanping@szu.edu.cn (PF), and zhigang.chen@usq.edu.au (ZGC); zhigang.chen@uq.edu.au (ZGC)

[#] Z.H. Zheng, X.L. Shi, and D.W. Ao contributed equally to this work.

Abstract

Owing to the earth-abundancy, eco-friendliness and high thermoelectric performance, $CoSb_3$ skutterudites have been employed in thermoelectric devices with a high energy conversion efficiency. However, the thermoelectric performance of $CoSb_3$-based thin films is still relatively low within the medium temperature range. In this work, we report a record high *ZT* of ~0.65 at 623 K in the n-type Ag/In co-doped $CoSb_3$ thin films, fabricated by a facile magnetron sputtering technique. Extensive characterizations and computational results indicate both Ag and In as fillers prefer to occupy the interstitial sites in the $CoSb_3$ lattice. A 0.2 % Ag doping induces impurity states in the band structure of $CoSb_3$, boosts the density-of-states near the Fermi level and enhances the absolute Seebeck coefficient up to ~198 μV K^{-1}. Simultaneously, a 4.2 % In doping further tunes the bandgap, increases the electrical conductivity up to ~75 S cm^{-1}, and contributes to an optimized power factor of ~2.94 μW cm^{-1} K^{-2} at 623 K. In addition, these interstitial dopants accompanying with dense grain boundaries contribute an ultra-low thermal conductivity of ~0.28 W m^{-1} K^{-1} at 623 K, leading to a high *ZT* in the film system. This work demonstrates that rational band engineering and structural manipulations can achieve high performance in n-type $CoSb_3$-based thin films, which possess full potential for applying to miniature thermoelectric devices.

Keywords: thermoelectric; $CoSb_3$; thin film; doping; characterization; calculation.

1. Introduction

Fossil fuels are typical non-renewable resources that provide most of the energy for human life. However, their consumption and depletion cause ever-growing environmental issues. Thermoelectric materials and devices can realize a direct conversion between heat and electricity, making them good candidates for tackling the above energy dilemma [1]. The

performance of thermoelectric materials is evaluated by the dimensionless figure-of-merit, $ZT = S^2\sigma T/\kappa = S^2\sigma T/(\kappa_e + \kappa_l)$, where S, σ, $S^2\sigma$, T, κ, κ_e, and κ_l are the Seebeck coefficient, electrical conductivity, power factor, absolute temperature, thermal conductivity, electronic thermal conductivity, and lattice thermal conductivity [2], respectively. A high $S^2\sigma$ and low κ are required to achieve a high ZT. Historically, rational band engineering was commonly used to optimize the $S^2\sigma$ by tuning the electrical transport properties (S and σ), and structural manipulations were employed to reduce the κ (mainly κ_l) [3]. Computational methods were also used to explore new thermoelectric materials with potentially high ZT values [4, 5].

To date, many thermoelectric materials have exhibited excellent thermoelectric performance with ZT values >1.5 [6], such as the p-type Hf-doped FeNbSb heavy-band half-Heusler alloys (ZT = ~1.5 at 1200 K) [7], p-type Na/Eu/Sn tri-doped PbTe (ZT = ~2.51 at 823 K) [8], p-type liquid-like $Cu_{1.94}Al_{0.02}Se$ (ZT = ~2.62 at 1029 K) [9], p-type Se-doped $AgSbTe_2$ (ZT = ~2.1 at 573 K) [10], p-type Pb/Bi co-doped GeTe (ZT = ~2.4 at 600 K) [11], p-type SnTe with CdTe coating on grains (ZT = ~1.9 at 929 K) [12], p-type $Bi_{0.5}Sb_{1.5}Te_3$ (ZT = ~1.86 at 320 K) [13], n-type Br-doped SnSe crystals (ZT = ~2.8 at 773 K) [14], n-type $Mg_{3.15}Mn_{0.05}Sb_{1.5}Bi_{0.49}Te_{0.01}$ zintls (ZT = ~1.85 at 723 K) [15], and n-type (Sr, Ba, Yb)$_y$$Co_4Sb_{12}$ skutterudites with 9.1 wt% $In_{0.4}Co_4Sb_{12}$ (ZT = ~1.8 at 823 K) [16]. Among these state-of-the-art thermoelectric materials, $CoSb_3$-based skutterudites have drawn significant attentions due to their suitable bandgap (~0.2 eV) [17], high stability [18], high cost-effectiveness [1], and environmentally friendly features [16]. Because of their outstanding thermoelectric performance and relatively high mechanical properties [1], $CoSb_3$-based skutterudites have been used in conventional thermoelectric devices as n-type “legs”, and a high energy conversion efficiency η of ~9.3 % can be realized at a temperature difference ΔT

of ~558 K in skutterudite-based thermoelectric modules [19], indicating their full potential for thermoelectric applications.

Recently, with the rapid development of portable and wearable electronics such as integrated circuits and micro-sensors, a low-dimensional power supply with a high power density and long service life is of significance to replace batteries for charging the microelectronic systems [20]. Miniature thermoelectric generators can generate electricity from the temperature difference between an electronic component and the surrounding environment [1], which possess significant potentials for portable and wearable electronics. To fabricate such miniature thermoelectric generators, thin-film-based thermoelectric materials are required [21, 22]. Compared with other thermoelectric thin film systems, $CoSb_3$-based skutterudites are good candidates due to their high-performance, low-toxic, high-stability, and mechanical robust features. To date, the p-type $CoSb_3$-based thin films have been explored with a promising *ZT* of 0.86 at 523 K by Ti-doping [23]. However, there is still a huge gap for achieving high-performance n-type $CoSb_3$-based thermoelectric thin films because only few works were reported with relatively low *ZT* of <0.5 [24], and their mechanisms for governing thermoelectric performance of thin films are still unclear [24-27]. Since both n-type and p-type materials are needed to assembly the miniature thermoelectric generators, exploring high-performance n-type $CoSb_3$-based thin films is of significance.

$CoSb_3$-based skutterudite materials have two natural interstitial sites in their lattices that can be filled by dopants [28], which provides a potential way to further improve their thermoelectric performance. In this work, we choose Ag and In as effective dopants to fill into $CoSb_3$ thin films using a facile magnetron sputtering technique. After comprehensive characterizations based on X-ray diffraction (XRD) and transmission electron microscopy (TEM), the Ag and In atoms are confirmed to be filled into the interstitial sites of $CoSb_3$,

acting as filling doping. First-principles density functional theory (DFT) calculations indicate that both Ag and In prefer to fill the interstitial sites rather than occupy the Co or Sb sites. Ag interstitial doping induces impurity band in $CoSb_3$ band structure and boost the *S*, and In further tunes the bandgap and leads significantly improved μ and σ, contributing to an optimized $S^2\sigma$. In addition, the induced Ag/In interstitial atoms act as point defects and the dense grain boundaries contribute to a reduction of κ, leading to a competitively high *ZT* of 0.65 at 623 K, which is a record high value for n-type $CoSb_3$-based thin films. This work demonstrates that high-performance $CoSb_3$-based thin solid films can be achieved by rational band engineering and structural manipulations.

2. Results and Discussions

In order to optimize the thermoelectric performance, we prepared $CoSb_3$-based thin films with different Ag and In doping concentrations on BK7 glass substrates. Extensive energy dispersive spectrometer (EDS) analysis was used to determine the real compositions of the films, and the EDS test for each specimen was repeated 20 times to reduce errors. Their thickness and compositional information are listed in **Table 1.** As shown in **Table 1**, all the prepared films have an atomic ratio of 0.36 for Co:Sb, which is slightly higher than the stoichiometric ratio of $CoSb_3$ suggesting Sb deficiency (Sb vacancies, V_{Sb}) in the films. Ag has a stable content of ~0.2 % for all the doped films, and the In contents were 3.3 %, 4.2 %, and 6.6 % for all the co-doped films. It should be noted that although electron probe microanalysis (EPMA) exhibits a higher accuracy than EDS for evaluating the composition, EPMA needs a certain depth to achieve a more accurate value. However, the thickness of our thin films was only ~200 nm, therefore it is not suitable for EPMA.

Table 1. Compositions and thicknesses of the as-fabricated thin films.

Thickness (nm)	Ag (at%)	In (at%)	Sb/Co
170	0	0	2.63
185	0.2±0.2	0	2.63
205	0.2±0.2	3.3±0.5	2.78
213	0.2±0.2	4.2±0.5	2.70
221	0.2±0.2	6.6±0.5	2.70

To carefully characterize the as-fabricated thin films, taking the 0.2 % Ag and 6.6 % In co-doped $CoSb_3$ thin film as an example, **Figure 1(a)** shows its optical image, from which the fabricated thin film shows typical metallic shining. **Figures 1(b)** is a typical scanning electron microscopy (SEM) image of the as-fabricated thin film, and **Figure 1(c)** is its cross-sectional SEM image with a uniform thickness of ~221.3 nm. **Figures 1(d-e)** show the EDS maps of the Ag/In co-doped $CoSb_3$ thin film surface. As can be seen, Ag, In, Co, and Sb are uniformly distributed, and no large Ag or In clusters can be found, indicating a homogeneous doping at a microscale. To further ensure that the structure and composition is uniform within the thickness of the film, **Figure 1(f)** shows a magnified cross-sectional TEM image of the thin film. It can be seen that the film is dense without delamination, confirming the homogeneity. **Figures 1(g-h)** show corresponding EDS maps. Clearly, Ag, In, Co, and Sb are uniformly distributed across the film, indicating a uniform distribution of the composition. Such a uniform composition can also be confirmed by the EDS scan lines, as shown in

Figure 1(i). The SEM images and EDS results of our fabricated $CoSb_3$ thin films with different Ag and In concentrations can be referred to **Figure S1** in the supporting information. Compared with the un-doped films, the doped thin films possess smooth and dense surfaces across the whole region, and no clusters or porous defects can be observed at the grain boundaries, which should be beneficial for the electrical transportation in our fabricated $CoSb_3$ thin films. In addition, with increasing Ag and In concentrations, larger grain sizes with shape-up morphology can be observed in the films.

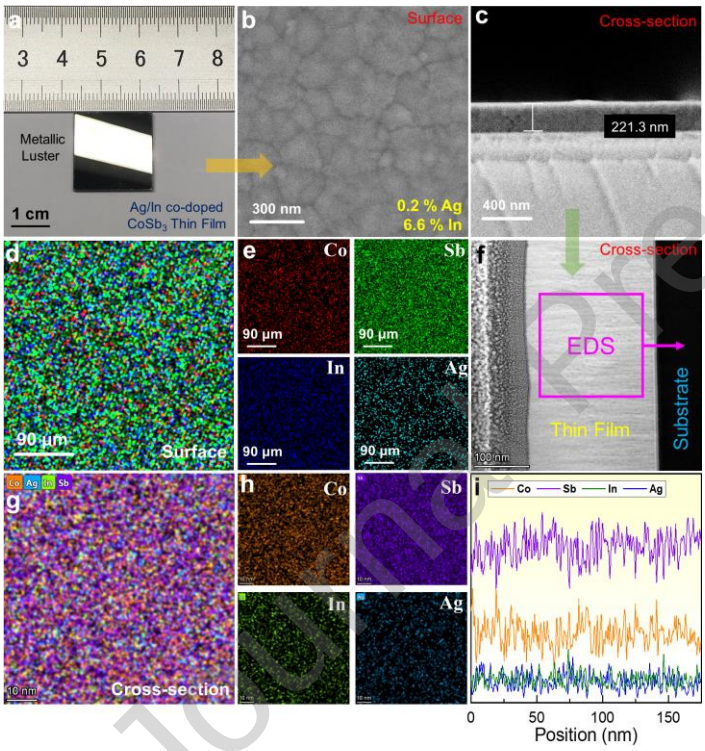

Figure 1. (a) Optical image, (b) scanning electron microscopy (SEM) image, and (c) cross-sectional SEM image of the Ag/In co-doped $CoSb_3$ thin solid film on a BK7 glass substrate fabricated by an advanced magnetron sputtering method. Here the doping concentrations of Ag and In are 0.2 % and 6.6 %, respectively. Energy dispersive spectrometer (EDS) maps for (d) total elements and (e) Ag, Sb, Co, and In of the Ag/In co-doped $CoSb_3$ thin film. (f) Magnified cross-sectional transmission electron microscopy (TEM) image of the Ag/In co-doped $CoSb_3$ thin film. EDS maps for (g) total elements and (h) Ag, Sb, Co, and In of the Ag/In co-doped $CoSb_3$ thin film taken from (f). (i) EDS scan lines for Ag, Sb, Co, and In of the Ag/In co-doped $CoSb_3$ thin film taken from (f).

To further study the doping behavior of In and Ag, **Figure 2(a)** shows XRD patterns of the as-fabricated $CoSb_3$ thin films with different Ag and In doping concentrations in a 2θ range from 10° to 80°. All the peaks can be indexed as $CoSb_3$ with a space group of Im3 (PDF#78-0976) [29]. No impurity phase can be observed within the detection limit of the XRD spectrometer, indicating all samples have a single $CoSb_3$ phase with a body-centered cubic skutterudite crystal structure. It should be noted that the volume fraction of the strongest peak corresponding to (013) plane was over 60 % of the whole pattern for all the films, suggesting a preferred orientation. According to the Debye–Sheerer equation [30], the estimated grain size of the un-doped and Ag single-doped films were ~23.4 nm and ~23.8 nm, and the grain size can be further increased to ~25.6 nm, 26.0 nm, and 27.6 nm after 3.3 %, 4.2 %, and 6.6 % In-doping, respectively. The rocking curves of (013) peaks are shown in **Figure 2(b)** tested in a θ range from 12° to 20°. The (013) peak of the un-doped $CoSb_3$ is 15.63°, and the peaks gradually shift to 15.44°, 15.34°, 15.26° and 15.06° after Ag doping, 3.3 %, 4.2 %, and 6.6 % In-doping, respectively. These results indicate that the peaks of the doped films progressively shift toward a small angle, suggesting an expansion of crystal cell. **Figure 2(c)** plots the determined lattice parameters as a function of actual Ag and In doping concentration. A non-linear expansion of lattice parameters can be observed, similar to previously reported filled $CoSb_3$ [31-33]. Such a non-linear expansion should be attributed to the doped elements that fill into the interstitial locations of the lattice [31], whereas the linear expansion related to solute concentration is only effective for the substitution of framework site atoms [34]. In addition, since the atomic radii of Ag (1.75 Å) and In (1.62Å) are larger than those of Co (1.27 Å) and Sb (1.38 Å), such a lattice expansion is understandable. The potential interstitial states of Ag and In are illustrate in the schematic crystal structure of Ag and In co-doped $CoSb_3$ (Inset of **Figure 2(c)**).

To further confirm the filling states of Ag and In, computational DFT calculations were performed. **Figure 2(d)** compares the calculated formation energies of Ag and In in different doping states using first-principles DFT method, which include occupying Co-sites, occupying Sb-sites, and interstitial state. The insets are the corresponding schematic crystal structures, and illustrate the corresponding occupied states. As can be seen, interstitial state possesses the lowest formation energy among the three situations for both Ag- and In-doping, suggesting that Ag and In prefer to occupy interstitial states in the lattice of $CoSb_3$. The reason for the formation of such a filling behavior can be further explained by the magnetron sputtering process. As schematically illustrated in **Figure 2(e)**, according to the sputtering thin film growth model [35], the atoms, that are first sputtered at the substrate, are usually self-assembled to form tiny island-like nanoparticles. Then, the subsequently sputtered atoms continue to grow around the formed islands. These grown islands connect each other to form a layer by the accumulation of atoms, as indicated by the atomic force microscope (AFM) images in **Figure 2(f)**. The deposited In layer has more island-shaped nucleation centers than the initial amorphous glass. When depositing Ag and $CoSb_3$ onto the In precursor layer, the $CoSb_3$ thin film grown on this island-shaped nucleation centers is larger than those on amorphous glass. This is consistent with the result of grain size.

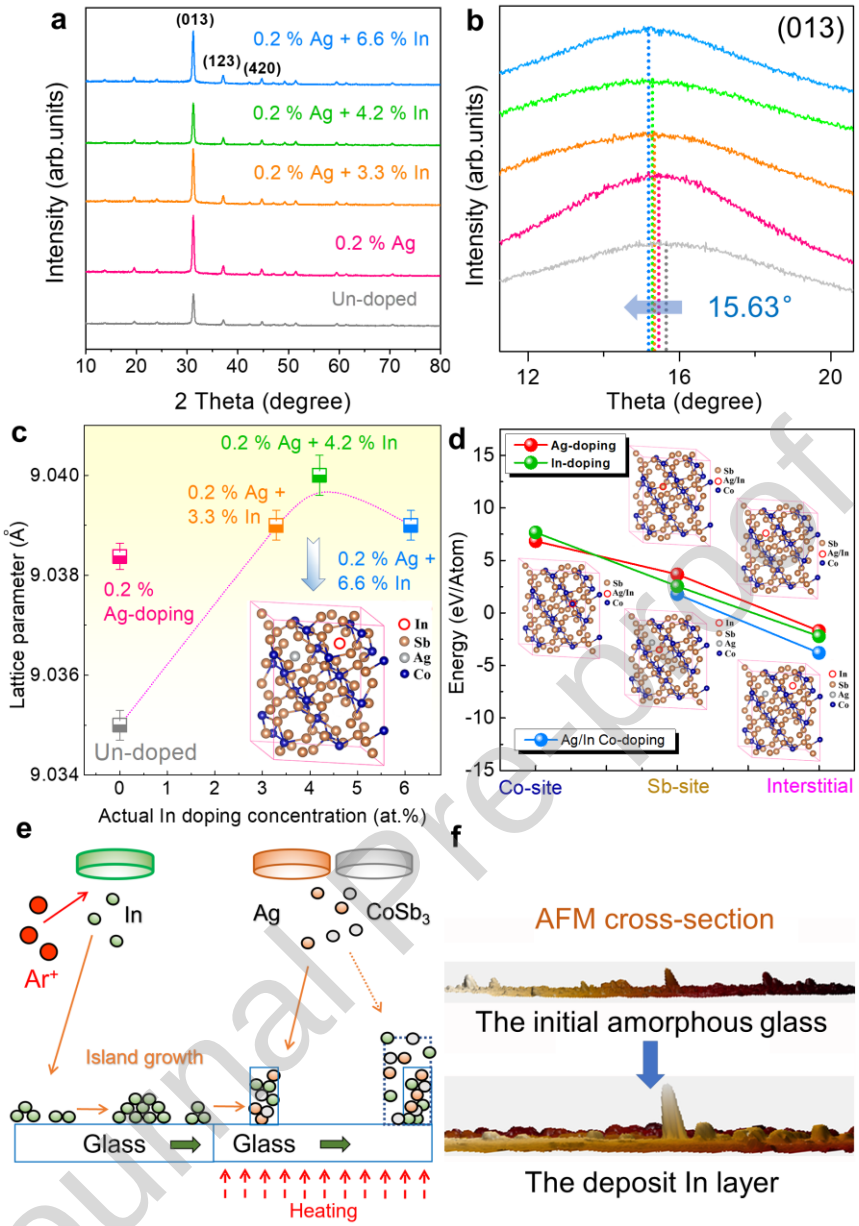

Figure 2. (a) X-ray diffraction (XRD) patterns of $CoSb_3$ thin films with different Ag and In doping concentrations in a 2θ range from 10° to 80°. (b) The rocking curve of (013) peak at 15.63° in a θ range from 12° to 20°. (c) Determined lattice parameters as a function of Ag and In doping concentration. The inset illustrates the potential interstitial states of Ag and In in $CoSb_3$. (d) Calculated formation energies of Ag and In in different doping states, including occupying Co-sites, occupying Sb-sites, and interstitial state. The insets illustrate the corresponding doping states. (e) Schematic diagram of fabrication of Ag/In co-doped $CoSb_3$ thin films, which is potentially responsible for the interstitial doping states of Ag and In found in $CoSb_3$. (f) The atomic force microscope (AFM) images of the initial amorphous glass and the deposited In layer.

To further study the doping behavior of Ag and In in our fabricated $CoSb_3$ thin films, extensive structural characterizations were carried out. **Figure 3(a)** shows a high-angle scanning transmission electron microscopy (STEM) annular dark-field imaging (HAADF) image of the 0.2 % Ag and 6.6 % In co-doped $CoSb_3$ thin film. The measured lattice spacings from the image are 2.86 Å and 2.41 Å, which correspond to the $CoSb_3$ crystal plane spacing of (013) and (123), respectively. In addition, obvious lattice distortion can also be observed, indicating the interstitial doping of Ag and In induces significant lattice strain. **Figure 3(b)** is an enlarge STEM-HAADF image and shows that vacancies (as the red rectangular marked area shows) can be observed, and **Figure 3(c)** is a magnified STEM-HAADF image that shows interstitial atoms (as the red dashed circles shows). These results confirm the existence of deficiency and interstitially doped atoms. To further confirm the positions of deficiency and interstitial atoms, Cs-corrected STEM-HAADF image of the Ag/In co-doped $CoSb_3$ thin film along the [001] direction is shown in **Figure 3(d)**. It is can be seen that a homogeneous and well-crystallized $CoSb_3$ film frame structure. **Figure 3(e)** presents the enlarged view of square frame from **Figure 3(d)**. The frame atom (Co and Sb) and the filler (Ag/In) atomic columns are clearly distinguished, and filler atoms (Ag/In) are randomly distributed in the interstitial sites of the frame of skutterudite. The intensity profile of the filler (Ag/In) and Sb atom from the long rectangular frame of **Figure 3(d)** is shown in **Figure 3(f)**. The intensity fluctuation between the neighbor Sb atom confirm that Ag/In as fillers occupy the interstitial sites in the $CoSb_3$ lattice.

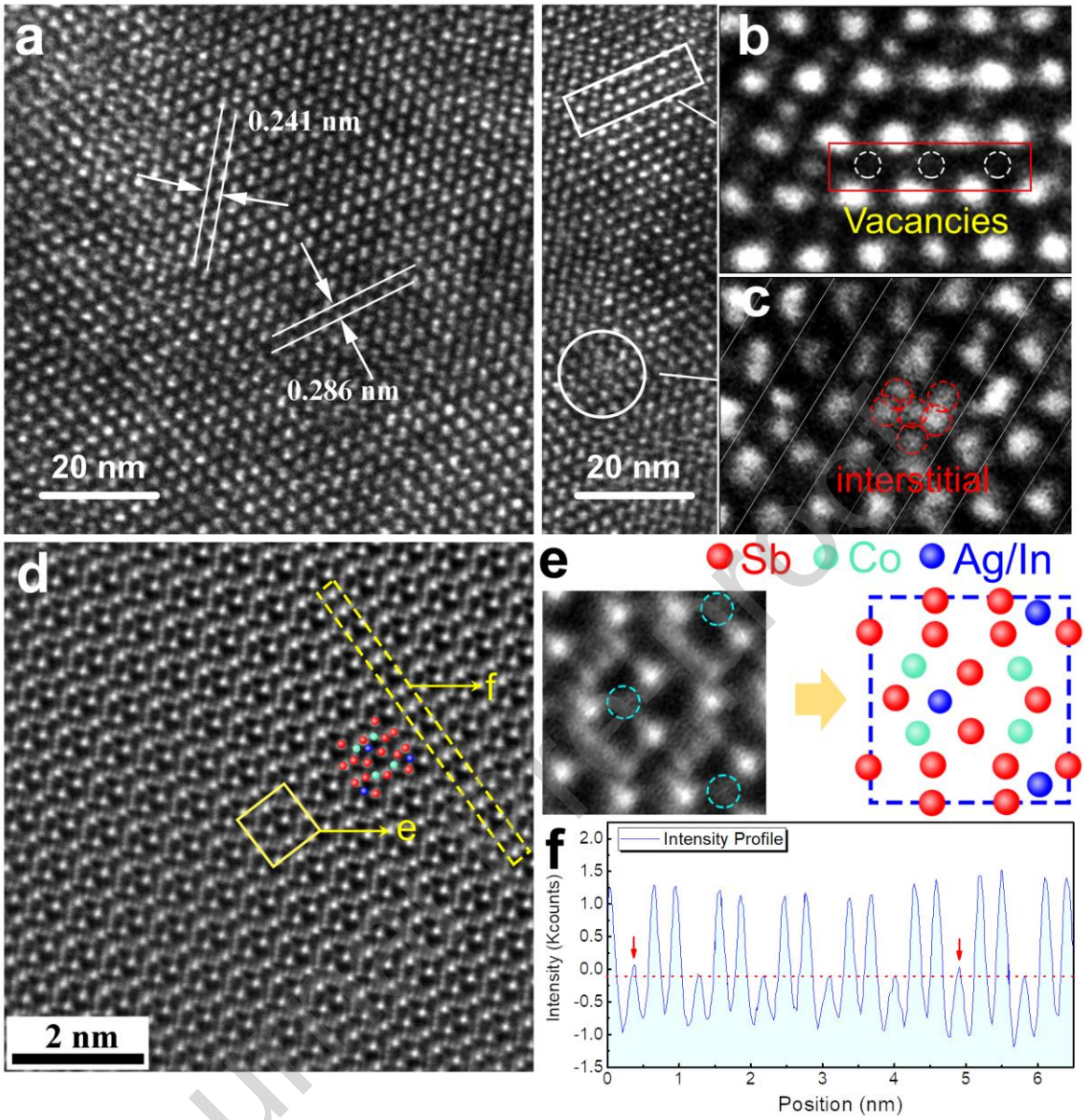

Figure 3. (a) STEM-HAADF image of the 0.2 % Ag and 6.6 % In co-doped $CoSb_3$ thin film, and corresponding magnified HAADF STEM images to show (b) Sb vacancies and (c) interstitial atoms. (d) Cs-correct STEM-HAADF image of 0.2 % Ag and 6.6 % In co-doped $CoSb_3$ thin films along the [001] direction. (e) Enlarged view of square frame and atomic arrangement in (d). (f) The intensity line profile scanning taken from the long rectangular frame in (d).

Figure 4(a) plots the measured temperature-dependent σ of our fabricated $CoSb_3$ thin films with different Ag and In doping concentrations. After doping with Ag, σ of the films is slightly increased at high temperatures (between 450 K and 623 K); while after further In-doping, σ is significantly increased within the entire temperature range, indicating that interstitial In-doping can effectively improve σ. A high σ of ~75 S cm^{-1} at 623 K can be observed in the 0.2 % Ag and 4.2 % In co-doped $CoSb_3$ film. **Figure 4(b)** shows the measured temperature-dependent S of our fabricated $CoSb_3$ thin films. The negative S values suggest a typical n-type behavior. Interestingly, Ag single-doping can achieve a highest absolute S up to 241.8 μV K^{-1}, indicating that Ag doping can significantly benefit S of $CoSb_3$. **Figure 4(c)** shows the measured optical bandgaps of the thin films using a UV/vis/NIR spectrophotometer. After Ag and In doping, the optical bandgap was increased, explaining the boosting of S. **Figure 4(d)** compares the measured room-temperature n and μ of $CoSb_3$ thin films as a function of Ag and In doping concentration. After Ag single-doping, n of the films is significantly reduced, which is responsible for the boosting of S; while with increasing the In-doping concentration, much higher μ can be achieved, despite that n is also reduced to some extent. The significantly enhanced μ is responsible for the improving of σ. **Figure 4(e)** compares the calculated room-temperature effective mass m^* and deformation potential E_{def} of $CoSb_3$ thin films as a function of Ag and In doping concentration. The m^* is firstly increased to a peak value after 0.2 % Ag doping, explaining the boosting of S. With increasing the In doping concentration, m^* is gradually decreased, indicating a reduction of S. The E_{def} is firstly reduced after 0.2 % Ag doping and then slightly increased with increasing the In doping concentration, explaining the enhancement of μ. As a result, an optimized $S^2\sigma$ of ~2.94 μW cm^{-1} K^{-2} at 623 K can be achieved in 0.2 % Ag and 4.2 % In co-doped $CoSb_3$ thin film, improved by ~100 % compared to that of the un-doped sample, as shown in **Figure 4(f)**. It should be noted that although the measured S and σ are distinct with different Ag and

In doping concentrations, the determined $S^2\sigma$ are much close, indicating that the achieved $S^2\sigma$ have been close to their optimized values due to the coupling of S and σ.

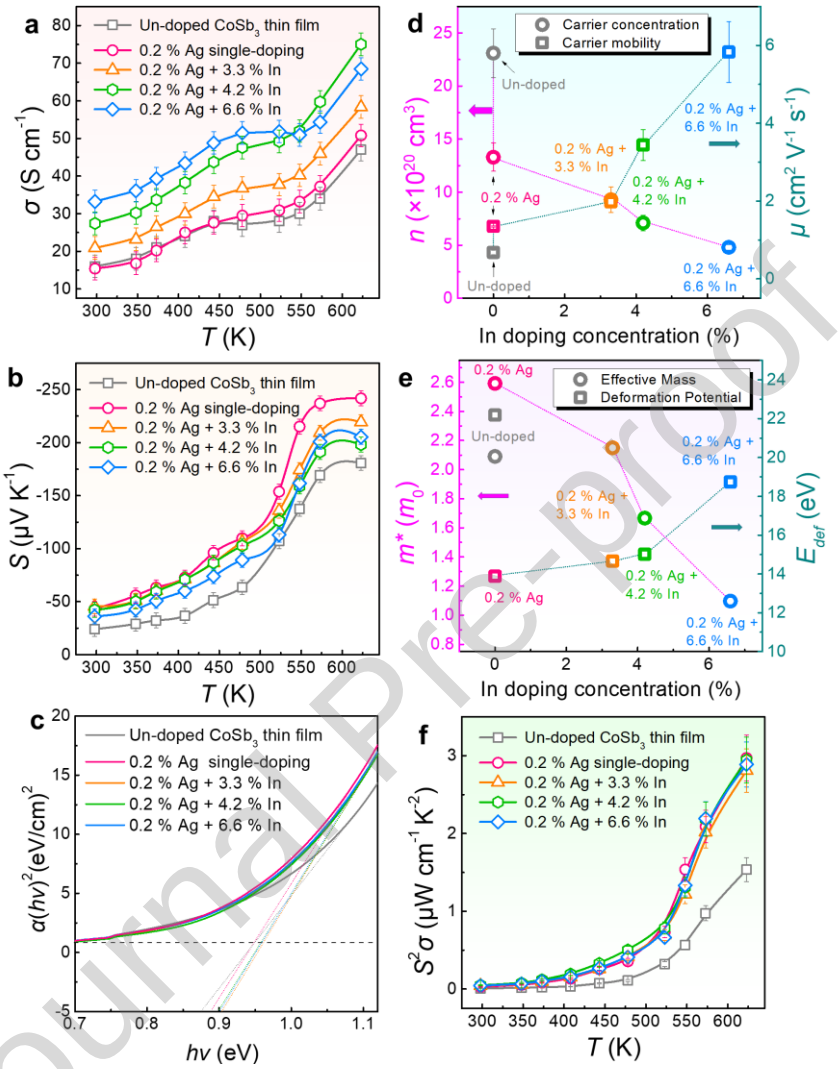

Figure 4. Measured temperature-dependent (a) σ and (b) S of as-fabricated $CoSb_3$ thin films with different Ag and In doping concentrations. (c) Measured optical bandgaps of $CoSb_3$ thin films. (d) Measured n and μ and (e) calculated m^* and E_{def} of $CoSb_3$ thin films as a function of In doping concentration. (f) Determined T-dependent $S^2\sigma$ of $CoSb_3$ thin films with different Ag and In doping concentrations.

To further explain the unique electrical transport performance of Ag/In co-doped $CoSb_3$ thin films, computational first-principles DFT calculations were investigated. **Figures 5(a-c)** show the calculated band structures and corresponding DOS of un-doped, interstitially Ag-doped, and interstitially Ag/In co-doped $CoSb_3$, respectively. The calculated bandgap values for un-doped, interstitially Ag-doped, and interstitially Ag/In co-doped $CoSb_3$ were 0.166 eV, 0.199 eV, and 0.206 eV, respectively. Clearly, In-doping increases the bandgap of $CoSb_3$, which have been verified in our optical spectroscopy measurement as shown in **Figure 4(c)**. Although DFT calculations are well known for the underestimation of bandgaps, we find that they predict the same trend as what we measured. The increased bandgap contributes to a rational coupling of S and σ and an optimized $S^2\sigma$. According to the formula deduced by Goldsmid and Sharp [36], $S_{max} = E_g/2qT_{max}$, where S_{max}, E_g, q, T_{max} is the absolute maximum value of S, band gap, elementary charge and temperature, respectively. The proportional relationship between S_{max} and E_g indicates that the Seebeck coefficient increases as the band gap increases [37]. As can be seen, Ag single-doping induces an impurity band and the highest peak of DOS near the Fermi level, which results in that the electrons at Fermi level more localize compared to the un-doped $CoSb_3$. Moreover, the enhancement of DOS near the Fermi level caused by impurity levels may lead to higher S values, which is in good agreement with the experimental results. It is worth mentioned that the increase in DOS caused by the impurity level may increase σ, but it will not affect n as the "normal" band. After inducing interstitial In, DOS near the Fermi level is more extended, resulting in higher σ.

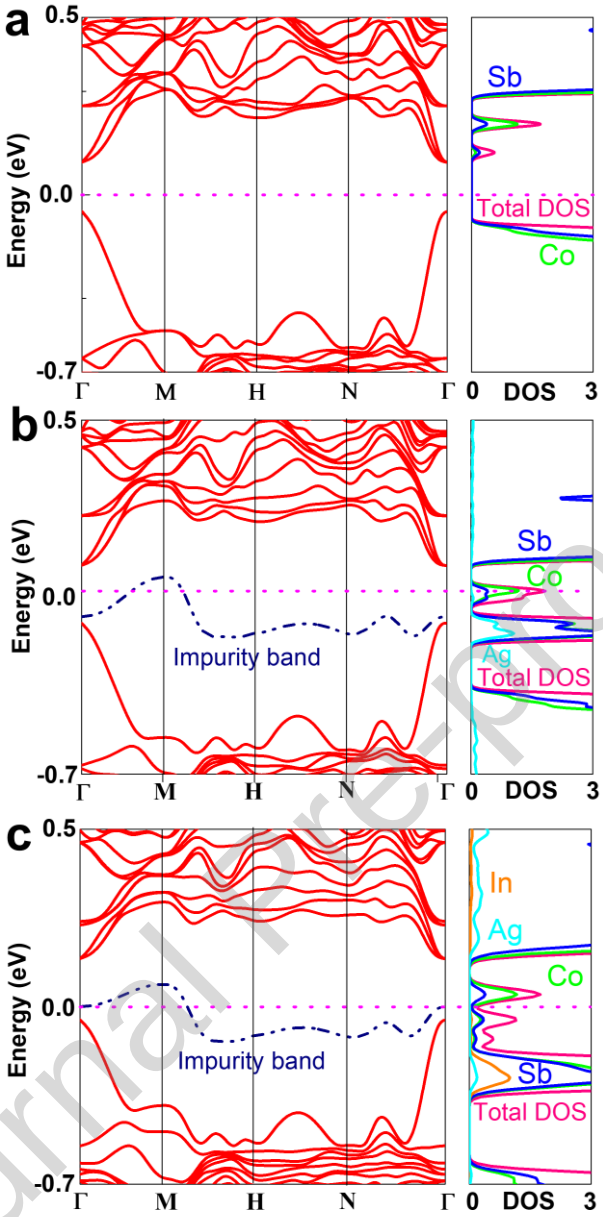

Figure 5. Calculated band structures and DOS of (a) un-doped, (b) interstitially Ag-doped, and (c) interstitially Ag/In co-doped $CoSb_3$.

We further measured thermal transport properties of our Ag/In co-doped $CoSb_3$ thin films. Because $CoSb_3$ has a typical cubic structure [38], the as-fabricated thin films can be treated as isotropy polycrystalline materials. The measured temperature-dependent κ with different Ag and In doping concentrations are plotted in **Figure 6(a)**. As can be seen, after doping with Ag and In, κ of the $CoSb_3$ thin films is significantly reduced. The minimized κ of ~0.28 W m^{-1} K^{-}

[1] at 623 K can be observed in the 0.2 % Ag and 4.2 % In co-doped $CoSb_3$ thin film. To explore the fundamental reason for the reduction of κ, both κ_e and κ_l were investigated. **Figure 6(b)** shows the determined *T*-dependent κ_e of $CoSb_3$ thin films with different Ag and In doping concentrations, which were calculated using Wiedemann–Franz law ($\kappa_e = L\sigma T$) [39], where *L* is the Lorenz number. The detailed calculated *L* values were calculated and can be referred in **Table S1** in Supporting Information. As can be seen, the achieved κ_e possesses the same trend of σ, but their values are much smaller than that of the corresponding κ, indicating that κ_l should dominate κ. **Figure 6(c)** shows temperature-dependent κ_l with different Ag and In doping concentrations. Clearly, the determined κ_l is much close to the corresponding κ, indicating that κ_l plays a significant role in determining the low κ of the films. **Figure 6(d)** compares κ_l of $CoSb_3$ thin films at 623 K as a function of Ag and In doping concentration. The insets illustrate the observed phonon scattering sources in the films, including the dense nano-grain boundaries that target to scatter the long-wavelength phonons, and Ag/In interstitial atoms and Sb vacancies as point defects that target to scatter the short-wavelength phonons, as observed in **Figure 3**. **Figure 6(e)** plots the determined temperature-dependent *ZT* of $CoSb_3$ thin films with different Ag and In doping concentrations. A competitively high *ZT* of 0.65 at 623 K is observed in 0.2 % Ag and 4.2 % In co-doped $CoSb_3$ thin film. **Figure 6(f)** compares the temperature-dependent *ZT* of our fabricated thin films with other state-of-the-art n-type thermoelectric films, including $SrTi_{0.8}Nb_{0.2}O_{2.75}$ using a pulsed laser deposition method [40], $Bi_2Te_{2.8}Se_{0.2}$ using a screen-printing method [41], $TiS_2[(HA)_{0.08}(H_2O)_{0.22}(DMSO)_{0.03}]$ using electrochemical intercalation and solvent exchange [42], and Yb-filled $CoSb_3$ using a DC-sputtering method [24]. **Table 2** summarizes the detailed information for the state-of-the-art n-type thermoelectric thin films reported in the last few years. As can be seen, our novel $CoSb_3$-based thin films possess a highly competitive *ZT* among the reported thin films at high temperature. Besides, our Ag/In

co-doped $CoSb_3$ thin films exhibit both high repeatability and stability in their thermoelectric performance, as shown in **Figure S3** and **S4**.

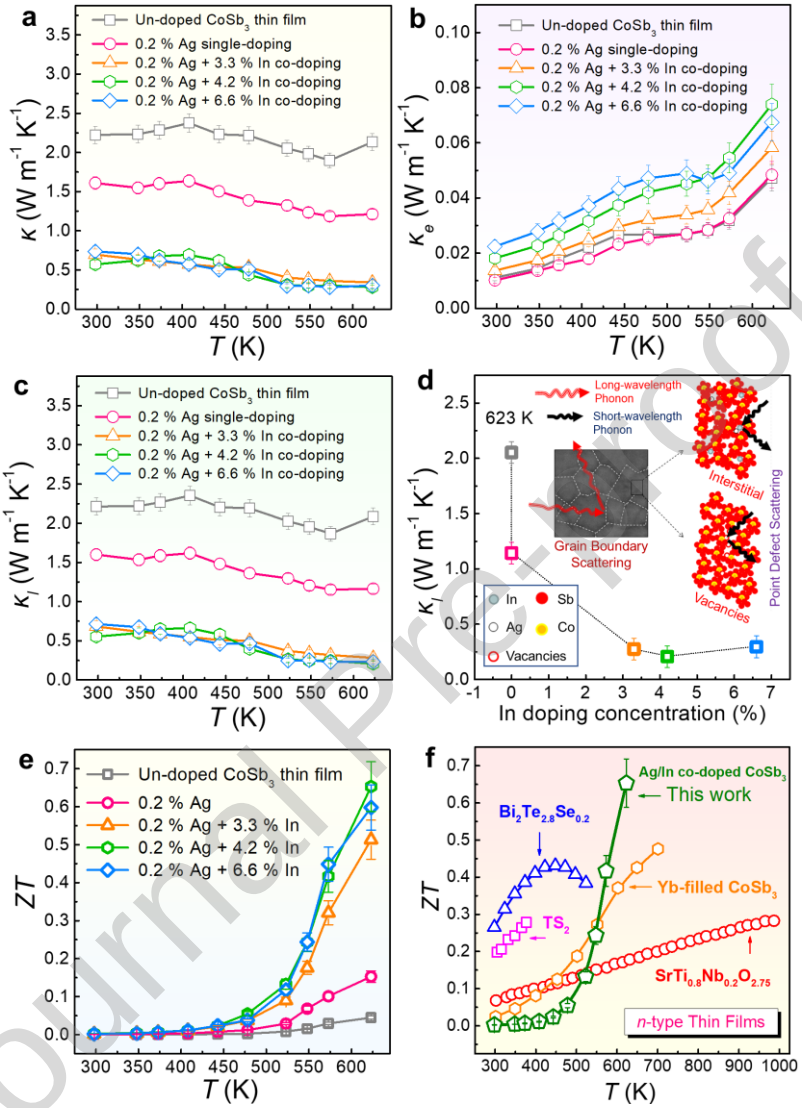

Figure 6. *T*-dependent (a) κ, (b) κ_e, and (c) κ_l of $CoSb_3$ thin films with different Ag and In doping concentrations. (d) κ_l of $CoSb_3$ thin films as a function of Ag and In doping concentration. The insets illustrate the observed phonon scattering sources in the films. (e) Determined *T*-dependent *ZT* of $CoSb_3$ thin films with different Ag and In doping concentrations. (f) Comparison of temperature *T*-dependent *ZT*s of various n-type thermoelectric thin films, including $SrTi_{0.8}Nb_{0.2}O_{2.75}$ using a pulsed laser deposition method [40], $Bi_2Te_{2.8}Se_{0.2}$ using a screen-printing method [41], $TiS_2[(HA)_{0.08}(H_2O)_{0.22}(DMSO)_{0.03}]$ using electrochemical intercalation and solvent exchange [42], Yb-filled $CoSb_3$ using a DC-sputtering method [24], and this work.

Table 2. A summary of n-type thermoelectric thin films.

Inorganic	**Substrate**	***ZT***	***T* (K)**	***σ* (S cm^{-1})**	***S* (μV K^{-1})**	***S*^{2}*σ* (μW cm^{-1} K^{-2})**	***κ* (W m^{-1} K^{-1})**	**Ref.**
Bi_2Te_3	Polyimide	~0.16	300	73.0	-137.8	~1.47	0.25	[43]
Bi_2Te_3	Glass fabric + PDMS	~0.33	298	~600.0	~-140.0	~11.8	~1.00	[44]
Bi_2Te_3 + RGO	Polyimide	0.0035	300	48.8	-148.0	1.08	-	[45]
$Bi_2Te_{2.8}Se_{0.2}$ nanoplates	Polyimide	0.43	448	275.0	-143.0	5.6	0.56	[41]
$Bi_2Se_3HA_{0.11}DMSO_{0.06}$	-	0.187	300	1480.0	-80.0	9.5	1.52	[46]
$Ag_2S_{0.5}Se_{0.45}Te_{0.05}$	-	0.44	300	270.0	-136.0	5.0	0.33	[47]
Ag_2Se	Polyimide	0.6	300	497.0	-140.0	9.874	0.478	[48]
$Ag_2Te_{0.6}S_{0.4}$	-	0.22	300	800.0	-84.0	5.67	0.78	[49]
$Sr_{0.95}La_{0.05}TiO_3$ nanocubes	Si (100)	0.2	273	160.0	-239.0	~9.1	1.50	[50]
$SrTi_{0.8}Nb_{0.2}O_3$	$LaAlO_3$	0.37	1000	~325.0	~-200.0	~13.0	~3.50	[51]
$SrTi_{0.8}Nb_{0.2}O_{2.75}$	$LaAlO_3$	0.29	1000	~614.2	~-125.4	~9.6	-	[40]
$SrTi_{0.8}Nb_{0.2}O_3$	Si, SiO_2	0.04	300	25.0	-156.0	~0.6	~0.45	[52]

CNTs	Glass	0.5	300	6.9	-1234.0	10.5	0.67	[53]
TiS_2	CaF	0.28	373	790.0	-75.5	4.5	0.12	[42]
Yb-filled $CoSb_3$	-	0.48	700	110.0	-260.0	~7.4	1.1	[24]
Ag/In co-doped $CoSb_3$, **this work**	-	0.65	623	75.0	~-198.0	~2.94	~0.28	

The thin films target to be applied in miniature thermoelectric devices. In this regard, the mechanical properties of the as-fabricated film are evaluated. **Figure 7** shows the measured elastic modulus E_r and the hardness H of $CoSb_3$ thin films with different Ag and In doping concentrations. Interestingly, after doping with Ag and In, both E_r and H were enhanced and mainly derived from the strengthening by interstitially doped heteroatoms. Such relatively high E_r of >100 GPa and H of >9 GPa significantly improve the stability of thin solid films when applying to miniature thermoelectric devices.

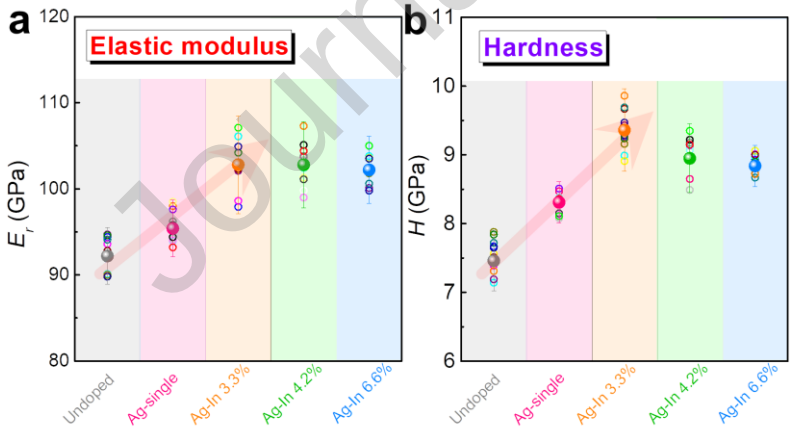

Figure 7. The measured (a) elastic modulus E_r and (b) the hardness H of $CoSb_3$ thin films with different Ag and In doping concentrations.

3. Conclusion

In this work, we fabricated n-type Ag/In co-doped $CoSb_3$-based thin solid films with a competitively high *ZT* of 0.65 at 623 K by using a facile magnetron sputtering technique. Both Ag and In prefer to occupy the interstitial sites in $CoSb_3$ as filling doping, confirmed by XRD and TEM based characterizations and first-principles DFT based calculations. Ag plays a significant role in boosting the *S* up to ~198 μV K^{-1}, and In further tunes the bandgap, increasing σ up to ~75 S cm^{-1} and contributing to an optimized $S^2\sigma$ of ~2.94 μW cm^{-1} K^{-2} at 623 K, improved by ~100 % compared to that of the un-doped sample. Furthermore, the induced Ag/In interstitial atoms as point defects and dense grain boundaries by nanostructuring act as phonon scattering centers, leading to an ultra-low κ of ~0.28 W m^{-1} K^{-1} at 623 K. This study indicate that a high-performance n-type $CoSb_3$-based thin solid films provide a new perspective for miniature thermoelectric device applications.

4. Experimental details

The experimental details are provided in the supporting information.

Acknowledgements

This work was supported by the National Natural Science Foundation of China (Grant No. 11604212), Guangdong Basic and Applied Basic Research Foundation (2020A1515010515), Shenzhen Key Lab Fund (ZDSYS 20170228105421966), Australia Research Council and Innovation Centre for Sustainable Steel Project. ZGC thanks the USQ Strategic research fund and USQ start-up grant. The authors thank Pro. S.F. Wang and Dr. H. Shuai for the testing thin film thermal conductivity. The authors are also thankful for the assistance on STEM-HAADF observation received from the Electron Microscope Center of the Shenzhen University.

Conflict of interest statement

There is no conflict of interest to be declared.

Reference

[1] X.-L. Shi, J. Zou, and Z.-G. Chen, Chem. Rev. 120 (2020) 7399-7515.

[2] M. Hong, W. Lyv, M. Li, S. Xu, Q. Sun, J. Zou, and Z.-G. Chen, Joule 4 (2020) 2030-2043.

[3] S. Xu, M. Hong, X.-L. Shi, M. Li, Q. Sun, Q. Chen, M. Dargusch, J. Zou, and Z.-G. Chen, Energy Environ. Sci. 13 (2020) 3480-3488.

[4] J. Yang, L. Xi, W. Qiu, L. Wu, X. Shi, L. Chen, J. Yang, W. Zhang, C. Uher, and D.J. Singh, npj Comput. Mater. 2 (2016) 15015.

[5] M. Hong, K. Zheng, W. Lyv, M. Li, X. Qu, Q. Sun, S. Xu, J. Zou, and Z.-G. Chen, Energy Environ. Sci. 13 (2020) 1856-1864.

[6] X.-L. Shi, W.-Y. Chen, X. Tao, J. Zou, and Z.-G. Chen, Mater. Horiz. (2020) DOI: 10.1039/D0MH00954G.

[7] C. Fu, S. Bai, Y. Liu, Y. Tang, L. Chen, X. Zhao, and T. Zhu, Nat. Commun. 6 (2015) 8144.

[8] Y. Wu, Z. Chen, P. Nan, F. Xiong, S. Lin, X. Zhang, Y. Chen, L. Chen, B. Ge, and Y. Pei, Joule 3 (2019) 1276-1288.

[9] B. Zhong, Y. Zhang, W. Li, Z. Chen, J. Cui, W. Li, Y. Xie, Q. Hao, and Q. He, Appl. Phys. Lett. 105 (2014) 123902.

[10] M. Hong, Z.G. Chen, L. Yang, Z.M. Liao, Y.C. Zou, Y.H. Chen, S. Matsumura, and J. Zou, Adv. Energy Mater. 8 (2017) 1702333.

[11] J. Li, X. Zhang, Z. Chen, S. Lin, W. Li, J. Shen, I.T. Witting, A. Faghaninia, Y. Chen, and A. Jain, Joule 2 (2018) 976-987.

[12] J. Hwang, H. Kim, M.-K. Han, J. Hong, J.-H. Shim, J.-Y. Tak, Y.S. Lim, Y. Jin, J. Kim, and H. Park, ACS Nano 13 (2019) 8347-8355.

[13] S.I. Kim, K.H. Lee, H.A. Mun, H.S. Kim, S.W. Hwang, J.W. Roh, D.J. Yang, W.H. Shin, X.S. Li, and Y.H. Lee, Science 348 (2015) 109-114.

[14] C. Chang, M. Wu, D. He, Y. Pei, C.-F. Wu, X. Wu, H. Yu, F. Zhu, K. Wang, and Y. Chen, Science 360 (2018) 778-783.

[15] X. Chen, H. Wu, J. Cui, Y. Xiao, Y. Zhang, J. He, Y. Chen, J. Cao, W. Cai, and S.J. Pennycook, Nano Energy 52 (2018) 246-255.

[16] G. Rogl, A. Grytsiv, K. Yubuta, S. Puchegger, E. Bauer, C. Raju, R. Mallik, and P. Rogl, Acta Mater. 95 (2015) 201-211.

[17] J. Zhang, B. Xu, L.-M. Wang, D. Yu, J. Yang, F. Yu, Z. Liu, J. He, B. Wen, and Y. Tian, Acta Mater. 60 (2012) 1246-1251.

[18] V. Ravi, S. Firdosy, T. Caillat, B. Lerch, A. Calamino, R. Pawlik, M. Nathal, A. Sechrist, J. Buchhalter, and S. Nutt, AIP Conf. Proc. 969 (2008) 656-662.

[19] Q. Zhang, Z. Zhou, M. Dylla, M.T. Agne, Y. Pei, L. Wang, Y. Tang, J. Liao, J. Li, and S. Bai, Nano Energy 41 (2017) 501-510.

[20] Y. Zhong, L. Zhang, V. Linseis, B. Qin, W. Chen, L.-D. Zhao, and H. Zhu, Nano Energy 72 (2020) 104742.

[21] D. Li, Y. Gong, Y. Chen, J. Lin, Q. Khan, Y. Zhang, Y. Li, H. Zhang, and H. Xie, Nano-Micro Lett. 12 (2020) 36.

[22] X.-L. Shi, H. Wu, Q. Liu, W. Zhou, S. Lu, Z. Shao, M. Dargusch, and Z.-G. Chen, Nano Energy 78 (2020) 105195.

[23] G.-x. Liang, Z.-h. Zheng, F. Li, J.-t. Luo, H. Jin, X.-h. Zhang, and P. Fan, J. Eur. Ceram. Soc. 39 (2019) 4842-4849.

[24] G. Fu, L. Zuo, J. Chen, M. Lu, and L. Yu, J. Appl. Phys. 117 (2015) 125304.

[25] M.V. Daniel, C. Brombacher, G. Beddies, N. Jöhrmann, M. Hietschold, D.C. Johnson, Z. Aabdin, N. Peranio, O. Eibl, and M. Albrecht, J. Alloys Compd. 624 (2015) 216-225.

[26] A. Ahmed and S. Han, J. Alloys Compd. 790 (2019) 577-586.

[27] S. Budak, C. Smith, C. Muntele, B. Chhay, K. Heidary, R.B. Johnson, and D. Ila, J. Intel. Mat. Syst. Str. 24 (2012) 1350-1356.

[28] Z. Liu, X. Meng, D. Qin, B. Cui, H. Wu, Y. Zhang, S.J. Pennycook, W. Cai, and J. Sui, J. Mater. Chem. C 7 (2019) 13622-13631.

[29] H. Sun, X. Jia, P. Lv, L. Deng, X. Guo, Y. Zhang, B. Sun, B. Liu, and H. Ma, RSC Adv. 5 (2015) 61324-61329.

[30] S. Amhil, E. choukri, S. Ben Moumen, A. Bourial, and L. Essaleh, Physica. B 556 (2019) 36-41.

[31] B.R. Ortiz, C.M. Crawford, R.W. McKinney, P.A. Parilla, and E.S. Toberer, J. Mater. Chem. A 4 (2016) 8444-8450.

[32] Y. Du, K.F. Cai, S. Chen, Z. Qin, and S.Z. Shen, J. Electron. Mater. 40 (2011) 1215-1220.

[33] T. He, J. Chen, H.D. Rosenfeld, and M.A. Subramanian, Chem. Mater. 18 (2006) 759-762.

[34] M. Beekman, E.N. Nenghabi, K. Biswas, C.W. Myles, M. Baitinger, Y. Grin, and G.S. Nolas, Inorg. Chem. 49 (2010) 5338-5340.

[35] P. Jood, G. Peleckis, X. Wang, and S.X. Dou, J. Mater. Res. 28 (2013) 1932-1939.

[36] H.J. Goldsmid and J.W. Sharp, J. Electron. Mater. 28 (1999) 869-872.

[37] K. Yamamoto, G. Narita, J. Yamasaki, and S. Iikubo, J. Phys. Chem. Solids 140 (2020) 109372.

[38] D.T. Morelli, T. Caillat, J.P. Fleurial, A. Borshchevsky, J. Vandersande, B. Chen, and C. Uher, Phys. Rev. B 51 (1995) 9622-9628.

[39] X.-L. Shi, X. Tao, J. Zou, and Z.-G. Chen, Adv. Sci. 7 (2020) 1902923.

[40] S.R.S. Kumar, A.Z. Barasheed, and H.N. Alshareef, ACS Appl. Mater. Interfaces 5 (2013) 7268-7273.

[41] T. Varghese, C. Hollar, J. Richardson, N. Kempf, C. Han, P. Gamarachchi, D. Estrada, R.J. Mehta, and Y. Zhang, Sci. Rep. 6 (2016) 33135.

[42] C. Wan, X. Gu, F. Dang, T. Itoh, Y. Wang, H. Sasaki, M. Kondo, K. Koga, K. Yabuki, and G.J. Snyder, Nat. Mater. 14 (2015) 622-627.

[43] J.H. We, S.J. Kim, and B.J. Cho, Energy 73 (2014) 506-512.

[44] S.J. Kim, J.H. We, and B.J. Cho, Energy Environ. Sci. 7 (2014) 1959-1965.

[45] B. Wu, Y. Guo, C. Hou, Q. Zhang, Y. Li, and H. Wang, Adv. Funct. Mater. 29 (2019) 1900304.

[46] P.-A. Zong, P. Zhang, S. Yin, Y. Huang, Y. Wang, and C. Wan, Adv. Electron. Mater. 5 (2019) 1800842.

[47] J. Liang, T. Wang, P. Qiu, S. Yang, C. Ming, H. Chen, Q. Song, K. Zhao, T.-R. Wei, D. Ren, Y.-Y. Sun, X. Shi, J. He, and L. Chen, Energy Environ. Sci. 12 (2019) 2983-2990.

[48] Y. Ding, Y. Qiu, K. Cai, Q. Yao, S. Chen, L. Chen, and J. He, Nat. Commun. 10 (2019) 841.

[49] S. He, Y. Li, L. Liu, Y. Jiang, J. Feng, W. Zhu, J. Zhang, Z. Dong, Y. Deng, J. Luo, W. Zhang, and G. Chen, Sci. Adv. 6 (2020) eaaz8423.

[50] F. Dang, C. Wan, N.-H. Park, K. Tsuruta, W.-S. Seo, and K. Koumoto, ACS Appl. Mater. Interfaces 5 (2013) 10933-10937.

[51] S. Ohta, T. Nomura, H. Ohta, M. Hirano, H. Hosono, and K. Koumoto, Appl. Phys. Lett. 87 (2005) 092108.

[52] C.-S. Park, M.-H. Hong, H.H. Cho, and H.-H. Park, J. Eur. Ceram. Soc. 38 (2018) 125-130.

[53] H. Wang, J.H. Hsu, S.I. Yi, S.L. Kim, K. Choi, G. Yang, and C. Yu, Adv. Mater. 27 (2015) 6855-6861.

Author Information

Zhuang-Hao Zheng received his PhD degree from University of Rennes 1, Rennes, France in 2018. He is an associate researcher in College of Physics and Optoelectronic Engineering, Shenzhen University, Shenzhen, China. His research interests include thermoelectric materials and devices, solar energy materials and solar cells. He published over 120 science citation index (SCI) journal papers in Advanced Materials, Nano Energy, Nanoscale, and other journals. He is regular journal paper reviewers for more than 20 journals.

Xiao-Lei Shi is currently a Research Fellow of Energy Materials at the University of Southern Queensland. He received his bachelor and master's degree in 2008 and 2011 from University of Science and Technology Beijing, respectively. He worked as an research and development engineer in Tsinghua University from 2012 to 2015, and received his Ph.D degree in 2019 from the University of Queensland. His researches focus on the development of high-performance thermoelectrics and underlying physics and chemistry.

Dong-Wei Ao received his Ph.D. degree from Shandong University, China in 2019. He works in College of Physics and Optoelectronic Engineering, Shenzhen University, China as a postdoctoral researcher. His main research areas are thermoelectric materials and devices.

Wei-Di Liu received his Ph.D. from the University of Queensland, Australia, in 2020. He is currently a research officer in the University of Queensland, Australia. His research interest lies in low-cost, eco-friendly thermoelectric materials.

Yue-Xing Chen is an assistant professor of College of Physics and Optoelectronic Engineering at Shenzhen University. He obtained his bachelor's degree at Fuzhou University in 2008. Later , he received his master's degree at University of Science and Technology Beijing in 2011. He received his Ph.D. degree from Hiroshima University in 2014. After working in Toyota Technological Institute and Southern University of Science and Technology as a postdoctor from 2014 to 2018, he joined Shenzhen University in 2018. His research interests focus on thermoelectric materials and crystal growth.

Fu Li is an assistant professor of College of Physics and Optoelectronic Engineering at Shenzhen University. She received her B.E. degree in Materials Science and Engineering from China University in Geosciences in 2008. And then, she joined Prof. Jing-Feng Li's group at Tsinghua University and obtained the Ph.D. degree in Materials Science and Engineering in 2013. After working in Graduate School at Shenzhen of Tsinghua University as a postdoctoral from 2013 to 2016, she joined Shenzhen University in 2016. Her research focuses on advanced thermoelectric materials and microdevices.

Shuo Chen is an assistant professor in College of Physics and Optoelectronic Engineering, Shenzhen University, China. He obtained his PhD degrees in Materials Science and Engineering from Zhejiang University, China, and Materials Science from University of Rennes 1, France. He focuses on the research of chalcogenide semiconductors, including the controllable synthesis of materials and applications as photoelectric devices.

Xiao-Qing Tian is an associate professor of the college of physics and optical engineering of Shenzhen University. He received his B.Sc. from Nanjing University in 2004 and M.Sc. from the Chinese Academy of Sciences in 2007 and Ph.D. from the Chinese University of Hong Kong in 2010. He is a visiting student of Princeton University and a visiting scholar of the Hong Kong University of Science and Technology. His research focus on the electronic, transport, magnetic and optical properties of solid states including traditional semiconductors, two-dimensional materials and alloys especially by the first-principles method.

Xin-Ru Li is an assistant professor of the college of physics and optical engineering of Shenzhen University. She received her B.Sc and Ph. D from Shandong University in 2012 and 2017. She was a postdoc researcher at Technische Universität Darmstadt, Germany. Her research focuses on high throughput calculations combined with first principles studies on electronic, magnetic or transport properties of two-dimensional functional materials.

Jing-Yi Duan majored in physics at Shenzhen University for his bachelor and master degrees, is currently enrolled in a PhD program in the Yao Group at Beijing Institute of Technology. Focusing on modulation of material properties, the author has published two articles with his supervisor in Advanced Functional Materials and Nanoscale respectively.

Hong-Li Ma has received her PhD degree at University of Rennes I in France in 1991 and she is research engineer at the CNRS, the French National center for scientific research. She is specialized in chalcogenide glasses and glass-ceramics essentially for infrared photonic application and more recently for energy conversion and storage. She is author or co-author of more than 150 scientific publications.

Xiang-Hua Zhang is research director of the French CNRS (National center of scientific research), working at University of Rennes I. He graduated from Zhejiang University, China and got his PhD degree at University of Rennes I, France. He became permanent researcher of the CNRS in 1989. In 1996, he was the founding president of Umicore IR glass. He went back to CNRS as research director in 2002. He is specialized in infrared transmitting glasses and ceramics for more than 35 years with 350 peer-reviewed publications.

Guang-Xing Liang is an associate researcher in College of Physics and Optoelectronic Engineering, Shenzhen University, Shenzhen, China. He obtained his PhD degree from University of Rennes 1, Rennes, France. He has extensive experience in solar energy materials and solar cells, including Sb2Se3, CZTS and perovskite, etc. He published over 120 science citation index (SCI) journal papers in Advanced Materials, Nano Energy, Chemical Engineering Journal, and other journals. He is regular journal paper reviewers for more than 20 journals. He is the academic editors of Advances in Materials Science and Engineering.

Ping Fan is a professor in College of Physics and Optoelectronic Engineering, Shenzhen University, China. He is the director of Shenzhen Key Laboratory of Advanced Thin Films and Applications and Shenzhen Vaccum Society. He received his PHD in Shanghai Institute of optical and Fine Mechanics Chinese Academy of Sciences, China, in 2005. He has published more than 100 SCI papers. His research interests include solar energy materials and solar cells, thermoelectric materials and devices. He is regular journal paper reviewers for more than 20 journals.

Zhi-Gang Chen is currently a Professor of Energy Materials in the University of Southern Queensland (USQ). He received his Ph.D in materials science and engineering from the Institute of Metal Research, Chinese Academy of Science, in 2008. After his Ph.D, he had worked at the University of Queensland for seven years before moving to USQ, in 2016. His research concentrates on smart functional materials for thermoelectrics and nanoelectronics from synthesizing materials to understanding their underlying physics and chemistry.

Graphical abstract

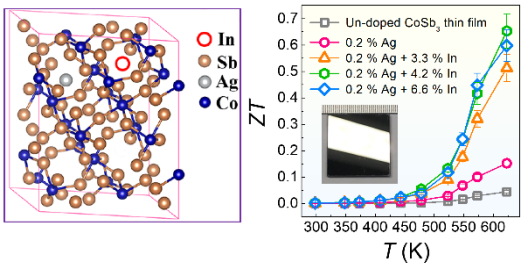

CRediT author statement

Zhuang-Hao Zheng: Conceptualization, Methodology, Validation, Formal analysis, Investigation, Data Curation, Writing - Original Draft;

Xiao-Lei Shi: Conceptualization, Methodology, Formal analysis, Investigation, Data Curation, Writing - Original Draft, Visualization;

Dong-Wei Ao: Conceptualization, Formal analysis, Resources, Data Curation;

Wei-Di Liu: Formal analysis;

Yue-Xing Chen: Formal analysis;

Fu Li: Conceptualization, Formal analysis, Resources;

Shuo Chen: Formal analysis;

Xiao-Qing Tian: Formal analysis;

Xin-Ru Li: Software;

Jing-Yi Duan: Formal analysis;

Hong-Li Ma: Formal analysis;

Xiang-Hua Zhang: Formal analysis;

Guang-Xing Liang: Software;

Ping Fan: Resources, Supervision, Project administration, Funding acquisition;

Zhi-Gang Chen: Conceptualization, Formal analysis, Writing - Review & Editing, Supervision, Project administration, Funding acquisition.

Declaration of interests

☒ The authors declare that they have no known competing financial interests or personal relationships that could have appeared to influence the work reported in this paper.

☐The authors declare the following financial interests/personal relationships which may be considered as potential competing interests:

Highlight

- A record high *ZT* of ~0.65 at 623 K is achieved in the n-type $CoSb_3$ thin films;
- Both Ag and In prefer to occupy the interstitial sites in the $CoSb_3$ lattice;
- Ag induces impurity states in the band structure, and In further tunes the bandgap;
- Interstitial dopants with dense grain boundaries contribute ultra-low thermal conductivities.
- Strengthened mechanical properties were realized by Ag/In co-doping.